Survival times of supramassive neutron stars resulting from binary neutron star mergers

Paz Beniamini[1,2]*, Wenbin Lu[1]

[1]*Theoretical Astrophysics, Walter Burke Institute for Theoretical Physics, Mail Code 350-17, Caltech, Pasadena, CA 91125, USA*
[2]*Astrophysics Research Center of the Open University (ARCO), The Open University of Israel, P.O Box 808, Ra'anana 43537, Israel*

6 April 2021

ABSTRACT

A binary neutron star (BNS) merger can lead to various outcomes, from indefinitely stable neutron stars, through supramassive (SMNS) or hypermassive (HMNS) neutron stars supported only temporarily against gravity, to black holes formed promptly after the merger. Up-to-date constraints on the BNS total mass and the neutron star equation of state suggest that a long-lived SMNS may form in $\sim 0.45 - 0.9$ of BNS mergers. We find that a SMNS typically needs to lose $\sim 3 - 6 \times 10^{52}$ erg of it's rotational energy before it collapses, on a fraction of the spin-down timescale. A SMNS formation imprints on the electromagnetic counterparts to the BNS merger. However, a comparison with observations reveals tensions. First, the distribution of collapse times is too wide and that of released energies too narrow (and the energy itself too large) to explain the observed distributions of internal X-ray plateaus, invoked as evidence for SMNS-powered energy injection. Secondly, the immense energy injection into the blastwave should lead to extremely bright radio transients which previous studies found to be inconsistent with deep radio observations of short gamma-ray bursts. Furthermore, we show that upcoming all-sky radio surveys will enable to constrain the distribution of extracted energies, independently of a GRB jet formation. Our results can be self-consistently understood, provided that BNS merger remnants collapse shortly after their formation (even if their masses are low enough to allow for SMNS formation). We briefly outline how this collapse may be achieved. Future simulations will be needed to test this hypothesis.

Key words: stars: neutron – gamma-ray burst: general – stars: jets

1 INTRODUCTION

The electromagnetic (EM) appearance of binary neutron star (BNS) mergers depend strongly on the nature and evolution of the post-merger remnant, which in turn depends on the component masses as well as the equation of state (EoS) of matter in the deep interior of neutron stars (NSs) (Shibata & Hotokezaka 2019). Numerical simulations of the gravitational wave (GW) driven dynamical merger process show that the initial remnant is supported against gravitational collapse by strong differential rotation and partially by thermal pressure (Shibata & Taniguchi 2006; Baiotti et al. 2008; Sekiguchi et al. 2011; Hotokezaka et al. 2013; Kiuchi et al. 2014; Kaplan et al. 2014). Subsequently, the system evolves on the viscous timescale that is roughly $\alpha^{-1} \lesssim 100$ times longer than the rotational period of ~ 1 ms, where the Shakura & Sunyaev (1973) dimensionless viscosity parameter is found to be $\alpha \gtrsim 10^{-2}$ in the outer envelope of the remnant NS as given by magneto-hydrodynamic (MHD) turbulence (Kiuchi et al. 2018). However, simulations have not been able to capture the full range of lengthscales and physical processes needed to understand the transport of angular momentum by e.g., Kelvin-Helmholtz and magneto-rotational instabilities (e.g., Kiuchi et al. 2014; Ciolfi et al. 2019). A simpler approach is to carry out (two-dimensional) viscous hydrodynamic simulations, under the assumption that sub-grid MHD processes operate efficiently to generate

a macroscopic viscosity (e.g., Shibata et al. 2017a; Radice 2017; Fujibayashi et al. 2018). It is found that the outer envelope viscously spreads into a torus, which contains $\sim 0.1 M_\odot$ and a large fraction of the angular momentum. However, the evolution of the rotational profile of the neutron star (e.g., how it approaches uniform rotation) and the share of angular momentum between the NS and the torus are highly uncertain as they depend sensitively on the choice of viscosity prescriptions. On longer timescales ~ 1 s, neutrino cooling removes thermal energy ($\sim 0.05 M_\odot c^2$), increases the central density of the NS, and may cause marginally stable systems to collapse. If at the end of this phase the NS has a sufficiently low mass and sufficiently high angular momentum, it will likely settle into uniform rotation, and become a supramassive neutron star (SMNS), supported against gravity by its fast rotation.

Observations of NSs near two solar masses in a number of sources (Demorest et al. 2010; Antoniadis et al. 2013; Cromartie et al. 2020) suggest that the pressure above nuclear saturation density of 2.8×10^{14} g cm^{-3} must be sufficiently high such that the maximum mass of non-rotating NSs, $M_{\max}$, is substantially greater than $2 M_\odot$ [1]. Centrifugal support due to uniform rotation allows the maximum mass to be up to about 20% higher than that of the non-rotating spherical configuration (e.g., Cook et al. 1994; Breu & Rezzolla

---

* E-mail: paz.beniamini@gmail.com

---

[1] It has been argued that electromagnetic observations of GW170817 place an upper limit of $M_{\max} \lesssim 2.3 M_\odot$ (Margalit & Metzger 2017; Granot et al. 2017; Shibata et al. 2017b; Rezzolla et al. 2018).

2016). This means that a fraction of BNS merger remnants, at least the ones[2] $\lesssim 2.4 M_\odot$ (and possibly even higher mass ones), could be spinning sufficiently rapidly as SMNSs, which undergo secular spin-down on longer timescales $\gg 1$ s.

Magnetic spin-down from a long-lived ($\gg 1$ s) SMNS or stable NS provides a powerful source of energy injection, which has an important impact on the EM counterparts of BNS mergers. For instance, the baryonic ejecta may be strongly heated by the non-thermal radiation from the pulsar wind nebulae and produce a UV-optical transient that is much brighter than the traditional radioactive-decay powered kilonova/macronova (Kasen & Bildsten 2010; Yu et al. 2013; Metzger & Piro 2014). The non-thermal radiation in the nebula may escape the ejecta when the bound-free optical depth is less than unity, generating X-ray emission at the level of the spin-down luminosity lasting for a spin-down time or until the SMNS collapses into a black hole (BH) (Zhang 2013; Metzger & Piro 2014). It has also been proposed that the long-lasting plateau seen in the X-ray lightcurve of some short gamma-ray bursts (GRBs) are produced by the nebula emission (Rowlinson et al. 2010; Metzger et al. 2011; Dall'Osso et al. 2011). On the other hand, the ejecta acquires a large kinetic energy comparable to the rotational energy of SMNS, and when decelerated by the surrounding medium, it produces bright multi-band afterglow emission (Gao et al. 2013; Metzger & Bower 2014).

In this paper, we study the distributions of the survival time and the emitted energy from SMNSs prior to the collapse. The goal is to make predictions based on known information (Galactic BNS statistics, LIGO observations, current EoS constraints; §2, 3) and then compare with observations (§4). We will show that these different components, brought together, reveal a tension. The implications which could provide insights onto the early stages of the merger remnant's evolution and its stability are discussed in §5.

2 METHOD

As we are interested in systems surviving for time-scales longer than the GRB prompt duration we focus on cold and uniformly rotating NSs, assuming that the differential rotation has subsided (on timescale of ~ 0.1 s) and neutrino cooling has ended (on timescale of ~ 1 s). We apply realistic equations of state (EOS) using the **rns** code (Stergioulas & Friedman 1995) [3] to simulate models of uniformly rotating cold NSs and consider different energy loss mechanisms. The latter is typically dominated by dipole spin-down which in turn depends on the magnetic field strength on the merger remnant's surface.

Our calculation proceeds as follows. We consider first the observed sample of 11 Galactic binary systems with well determined individual gravitational masses (listed in table 1) to simulate (gravitational) chirp masses and secondary to primary mass ratios: $M_{\rm ch}, q \equiv M_2/M_1 \leq 1$ according to observations. The observed sample can be described by independent distributions. $M_{\rm Ch}$ is fit by a normal distribution with $\mu_{M_{\rm Ch}} = 1.175 M_\odot, \sigma_{M_{\rm Ch}} = 0.044 M_\odot$. The parameter $\tilde{q} = (1-q)/q$ can be fit with an exponential distribution with $\lambda_{\tilde{q}} = 0.0954$. This description ensures that $0 \leq q \leq 1$. $M_{\rm ch}, q$

are used to calculate M_1, M_2 according to

$$M_1 = M_{\rm Ch} q^{-3/5}(1+q)^{1/5} \quad , \quad M_2 = q M_1 \qquad (1)$$

While the directly measured quantity for an individual NS is its gravitational mass, it is useful to consider the equivalent baryonic mass, as the total baryonic mass is conserved during the merger. The gravitational masses M_1, M_2 are converted to baryonic masses $M_{1,0}, M_{2,0}$ using the assumed EoS, under the assumption of zero spin for the individual NSs (this is consistent with the rotation frequencies of Galactic BNS pulsars, which are well below break-up). During the merger, some of the mass is ejected in the form of dynamical ejecta and disk winds. We use the estimates for the (baryonic) mass of the ejecta, $M_{\rm ej,0}$, as a function of $M_{\rm ch}, q$ given by Margalit & Metzger (2019); Coughlin et al. (2019) based on fits to numerical relativity simulations. The baryonic mass of the remnant is then simply given by $M_0 = M_{1,0} + M_{2,0} - M_{\rm ej,0}$.

For a given EoS, we find the maximum baryonic mass of a non-rotating star, $M_{\rm max,0}$ and of a star rotating at the mass shedding limit, $M_{\rm th,0}$. For a given M_0, there are three possibilities. First, $M_0 > M_{\rm th,0}$. This leads to either a hypermassive neutron star (HMNS), supported only by differential rotation and / or thermal pressure or, for still higher masses, to a prompt collapse. In either case, the result is a very short survival time (assumed below to be ~ 0.1 s). The second possibility is $M_0 < M_{\rm max,0}$. In this case the NS is infinitely stable. The third case is obtained for $M_{\rm max,0} < M_0 < M_{\rm th,0}$. This is an interesting case, resulting in a finite survival time that we describe in more detail next.

For $M_{\rm max,0} < M_0 < M_{\rm th,0}$ we construct NS models with the specified EoS such that they have a constant baryonic mass, M_0 and different rotation rates. We also calculate the maximum extractable energy $E_{\rm ext} = E_{\Omega,\max}(M_0) - E_{\Omega,\min}(M_0)$ (see also Metzger et al. 2015a), which is the rotational energy that the NS can lose before it is forced to collapse ($E_{\Omega,\max}(M_0)$ is the rotational energy of a maximally rotating NS with baryonic mass M_0 and $E_{\Omega,\min}(M_0)$ is the minimum rotational energy required for this NS to support itself against collapse). An example of a track with constant baryonic mass in the plane of gravitational mass and rotational energy is shown in Fig. 1. As a limiting case we assume first that the remnant begins maximally rotating (i.e. at the mass shedding limit, Giacomazzo & Perna 2013). This is conservative, as lower initial rotation speeds will lead to a quicker collapse and less SMNSs. This second possibility, that the remnant losses a significant amount of its rotational energy while it is differentially rotating is explored in §3.1, in which we consider an SMNS that enters the cold uniform rotation stage with its rotational energy reduced to $0.5 E_{\Omega,\max}(M_0)$. Such a situation is in line with the general-relativistic magnetohydrodynamics (GRMHD) simulations by Ciolfi et al. (2019).

The remnant then spins down according to magnetic dipole radiation, $\dot{E}_{\rm D}$ and gravitational quadrupole radiation, $\dot{E}_{\rm G}$,

$$\dot{E}_\Omega = I\Omega\dot{\Omega} + 0.5\dot{I}\Omega^2 = \dot{E}_{\rm D} + \dot{E}_{\rm G} \qquad (2)$$

$$\dot{E}_{\rm D} = -\frac{B^2 R^6 \Omega^4}{6c^3} \qquad (3)$$

$$\dot{E}_{\rm G} = -\frac{32 I^2 \epsilon^2 G \Omega^6}{5c^5}. \qquad (4)$$

Where I is the NS moment of inertia, Ω is its spin frequency, B is the surface strength of the magnetic field, we have assumed an aligned rotator for $\dot{E}_{\rm D}$ and ϵ is the fractional deformation of the NS. The latter can be dominated by different physical effects. One specific deformation mechanism is due to the magnetic field, and given by

$$\epsilon = \beta \frac{R^4 B^2}{GM^2} \qquad (5)$$

---

[2] For instance, the PSR J1946+2052 BNS system (total mass $2.5 \pm 0.04 M_\odot$, Stovall et al. 2018), are expected to produce a SMNS, after accounting for mass loss of a few percent $M_\odot$ or more due to baryonic kilonova ejecta (e.g., Radice et al. 2018b) and then $\sim 0.1 M_\odot$ from GW and neutrinos (Hotokezaka et al. 2013; Bernuzzi et al. 2016).

[3] http://www.gravity.phys.uwm.edu/rns/

Table 1. Galactic binary neutron stars with well determined individual masses. To be consistent with the notation adopted in §2, we denote by M_1 the more massive of the NSs in the binary. This should not be confused with a standard notation in binary pulsar literature, by which M_1, M_2 are used to distinguish the observed pulsar from its companion.

System	$M_1 [M_\odot]$	$M_2 [M_\odot]$	reference
J0737-3039	1.338	1.249	Kramer et al. (2006)
J1906+0746	1.323	1.291	Lorimer et al. (2006)
J1756-2251	1.341	1.23	Faulkner et al. (2005)
B1913+16	1.44	1.389	Weisberg et al. (2010)
B1534+12	1.346	1.333	Stairs et al. (2002)
J1829+2456	1.306	1.299	Champion et al. (2005)
J1518+4904	1.41	1.31	Janssen et al. (2008)
J0453+1559	1.559	1.174	Martinez et al. (2015)
J1913+1102	1.62	1.27	Lazarus et al. (2016)
J1757-1854	1.3946	1.338	Cameron et al. (2018)
J0509+3801	1.46	1.34	Lynch et al. (2018)

where M is the gravitational mass of the NS remnant and $\beta \ll 1$ (we assume $\beta = 0.1$ below). The values of R, M, I depend in general on both the (fixed) M_0 and the (evolving) spin rate and are estimated directly from the rns models at each time step. Ω is evolved according to Eq. 2 until the amount of extracted energy equals E_{ext} and the NS collapses. The time elapsed by this point is denoted t_{survive}. This calculation is repeated 10^4 times (each time drawing different parameters from the chirp mass and mass ratio distributions), in order to obtain the distribution of $t_{\text{survive}}, E_{\text{ext}}$ values consistent with Galactic BNS systems.

3 RESULTS

In figure 2 we show the distribution of extracted energies and survival times for different EoS and different surface magnetic field strengths. We consider in particular the SLy EoS (Douchin & Haensel 2001) which is consistent with available observational constraints on the mass-radius curve of NSs (Coughlin et al. 2019). As a comparison case, we consider also the WFF2 EoS (Wiringa et al. 1988). The maximum masses of non-rotating NSs with these EoSs are $M_{\text{max}} = 2.05$ (SLy) and $M_{\text{max}} = 2.2$ (WFF2). These EoSs therefore bracket the allowed range of maximum masses allowed by observations. A large fraction ($\sim 45 - 90\%$) of the merger remnant population have baryonic masses in the range $M_{\text{max},0} < M_0 < M_{\text{th},0}$ which, in case the remnants begin as maximally rotating, correspond to formation of SMNSs and finite survival times. The median survival time under these assumptions is 80 s (330 s) for $B = 10^{15}$ G and SLy (WFF2) [0.9 s (3.5 s) for $B = 10^{16}$ G and SLy (WFF2)]. Approximately these times are $\sim 0.35\tau_{\text{D},0}$ (where $\tau_{\text{D},0}$ is the initial magnetic dipole spin-down time). This reflects the fact that the NS typically needs to lose ~ 0.35 of its rotational energy before collapsing, and for $t \ll \tau_{\text{D},0}$ the evolution of the rotational energy is approximately $E_\Omega \approx E_{\Omega,0}(1 - t/\tau_{\text{D},0})$ (assuming GW quadrupole radiation to be negligible, which is found to be the case in these calculations, even if we consider an extreme value of $\beta = 1$).

As mentioned above, the merger remnant must lose a large fraction of its initial rotational energy, with a median loss of $\sim 3 \times 10^{52}$ erg for the SLy EoS ($\sim 6 \times 10^{52}$ erg for the WFF2 EoS) before collapsing and with narrow deviations around those values ($\sigma_{\log_{10} E_{\text{ext}}} \approx 0.24$ in both cases). This huge amount of energy is much larger than that of the (collimation corrected) GRB jet or that of sub-relativistic ejecta powering the kilonova emission. As a result, a large fraction of this energy could be absorbed by the ejecta and dominate its kinetic
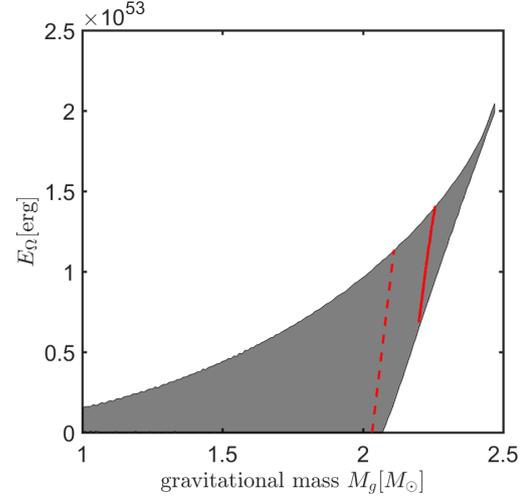

Figure 1. The shaded region depicts allowed solutions (confined by the energy at the mass shedding limit from above and by the minimum required energy for solid rotation from below) for cold uniformly rotating NSs in the plane of gravitational mass and NS rotational energy. The red solid (dashed) line represents a constant baryonic mass of $M_0 = 2.6 M_\odot$ ($M_0 = 2.4 M_\odot$), corresponding to a gravitational mass of $M_g = 2.26 M_\odot$ ($M_g = 2.11 M_\odot$) at the mass shedding limit. Results shown here are for the SLy EoS (Douchin & Haensel 2001).

energy budget at late times. Such large amounts of kinetic energy can be seen as strong radio emitters on timescales of years to tens of years, as addressed in more detail in §4.2.

Interestingly, even for a fixed magnetic field strength across different systems, the distribution of t_{survive} for SMNSs is very wide, with $\sigma_{\log_{10} t_{\text{survive}}} \approx 0.5$. Any spread in the surface field strength of the merger remnant (which is very natural), would only cause the distribution of t_{survive} to be much wider still. We return to this point in §4.1.

3.1 Slower initial rotations and fallback accretion

As mentioned in §2, GRMHD simulations point towards the possibility that the merger remnant losses a significant fraction of its initial rotation energy during the differential rotation phase (Kiuchi et al. 2018; Ciolfi et al. 2019). The energy lost at this phase is mostly converted to internal energy of the remnant. Following the results of Ciolfi et al. (2019), we consider here the possibility that the merger remnant enters the cold uniform rotation phase with a rotational energy of $0.5 E_{\Omega,\text{max}}(M_0)$. We note that the physical processes responsible for the angular momentum transport in the differential rotation phase are still highly uncertain. Radice et al. (2018a) argued that the total angular momentum of the merger remnant often exceeds the mass-shedding limit for SMNS (favoring the $E_\Omega = E_{\Omega,\text{max}}$ prescription considered earlier), but their simulations did not include an explicit treatment of angular momentum transport after the GW-driven dynamical merger phase.

We show in figure 3 the distributions of energies extracted and survival times prior to collapse for this case of slower initial rotation. The main difference compared to the case in which the merger remnant is born rotating at the mass shedding limit, is the fraction of systems that end up as SMNSs. This fraction is 2% (25%) for the SLy (WFF2) EoS. The implication is that, depending on the EoS, considering realistic estimates for the angular momentum loss during the differential rotation phase it is possible that only a very small
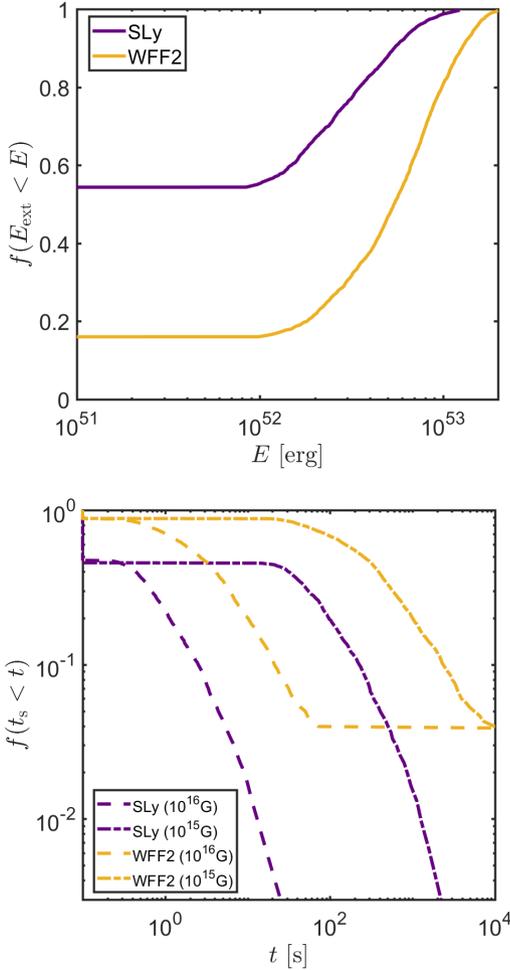
Figure 2. Cumulative distribution of the energies extracted (top) and survival times (bottom) of BNS merger remnants before they collapse to black holes. Results are calculated under the assumption that the merger remnant is born rotating at the mass shedding limit and shown for different EoS and, in the lower panel, for different surface field strengths.
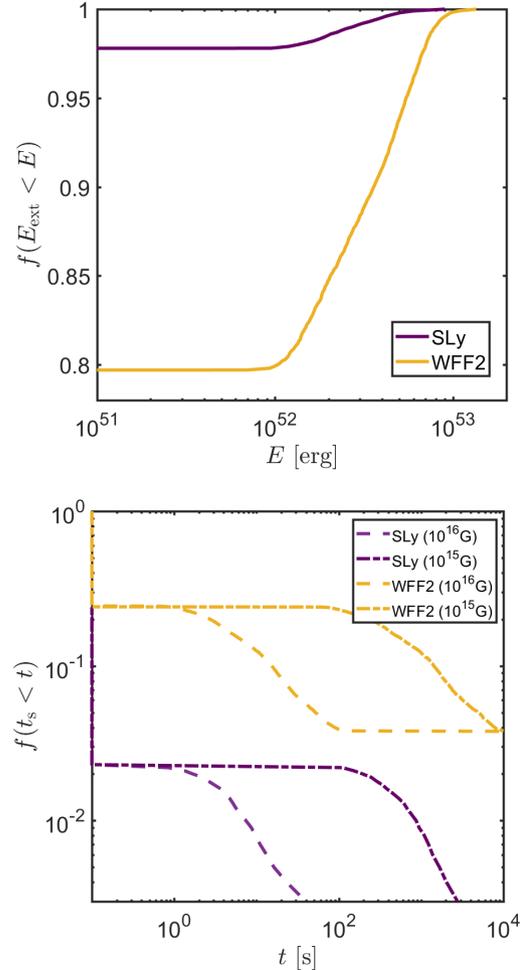
Figure 3. Same as Figure 2, but assuming that the NS merger remnant enters the cold uniform rotation phase with a rotational energy equaling $0.5E_{\Omega,\max}(M_0)$ (note the different scale for the energy plot as compared to Figure 2).

fraction, and perhaps even none of the merger remnants, result in long lived NSs.

The survival time and extracted energy distributions can also be modified in the presence of significant fallback accretion onto the newly born strongly magnetized NS — or magnetar (Metzger et al. 2018). In particular, the magnetar may transfer some of its angular momentum to the fallback disk, and as a result, spin down to the point of collapse after having released a smaller amount of its initial rotational energy. Metzger et al. (2018) have found that this can decrease the amount of energy released prior to collapse by up to a factor of a few. Similar to the case of slow initial rotation, this will lead to a faster collapse relative to the case of fast initial rotation with no fallback accretion.

4   COMPARISON WITH SGRBS AND IMPLICATIONS

4.1   Can magnetars power the observed plateaus?

X-ray afterglows of sGRBs sometimes exhibit a 'plateau' phase, where the emission is almost steady or declining very slowly with time. Previous studies (Zhang & Mészáros 2001; Rowlinson et al.

2010; Metzger et al. 2011; Dall'Osso et al. 2011; Rezzolla & Kumar 2015) have interpreted these as possible evidence of energy injection into the GRB jet with a duration comparable to the observed plateau (although see Eichler & Granot 2006; Granot et al. 2006; Ioka et al. 2006; Genet et al. 2007; Shen & Matzner 2012; Beniamini et al. 2020a; Oganesyan et al. 2020 for other interpretations). These studies pointed to a magnetar's spin-down as a possible source of this energy injection. Our results shed light on the viability of this interpretation.

Two types of plateaus are observed in sGRBs. The first are 'external plateaus'. These are plateaus in which the light-curve smoothly and gradually transitions from a flat temporal evolution to a declining one. More quantitatively, these are cases where the plateau declines on a timescale Δt such that $\Delta t/t \sim 1$ (where t is the time since the GRB trigger of the end of the plateau). These plateaus are dubbed external, since their low level of variability can be reproduced by emission from the external shock (the same region from which the standard afterglow signal is observed). As such it is not possible to separate by these lightcurves between a scenario where energy injection ended abruptly but the energy was then reprocessed at the external shock to a situation where the energy injection itself was simply slow to fade at the end of the plateau phase. Furthermore,

as mentioned above, such plateaus do not necessarily require any energy injection whatsoever.

The second type of plateaus are 'internal plateaus' in which the emission quickly declines at the end of the plateau (such that $\Delta t/t \ll 1$ with the same definitions as above). In these cases, the rapid variability strongly suggests energy injection as well as an emission radius well below the external shock. In the context of magnetar energy injection, the source of the abrupt cut-off is most naturally associated with the collapse of an unstable magnetar to a black hole.

Gompertz et al. (2020) study a sample of *Swift* detected sGRBs with known redshifts. Only 5/39 of the bursts in the sample exhibited an internal plateau. This is very low, as compared with the fraction $\approx 0.45 - 0.9$ of long lived SMNSs expected to result from neutron star mergers found above. Furthermore, the (source frame) durations of these internal plateaus are tightly clustered, with $< \log_{10} t_{IXP}[s] >= 2.15$, $\sigma_{\log_{10}(t_{IXP})} = 0.16$. As mentioned in §3, this is in contradiction with even the most conservative estimates for the deviation in $t_{survive}$, which is expected to span a wide range of survival times (this is true also in the case where the merger remnant enters the uniform rotation phase with a slower angular velocity and in the case where it undergoes significant fallback accretion early on). This is demonstrated in figure 4, where we show the survival time as a function of the remnant's dipole field strength and gravitational mass (measured immediately after collapse), under the assumption that the merger remnant is initially rotating at the mass shedding limit. The resulting survival times, span over five orders of magnitude, while the durations of internal plateaus all reside in a narrow strip within this plane. This makes the association of these plateaus with spin-down of SMNS extremely fine tuned. It is also worthwhile to stress that sGRBs with internal plateaus span a range of prompt gamma-ray energies, durations and redshifts consistent with the rest of the sGRB population (see Gompertz et al. 2020), suggesting that observational selection effects are unlikely to play a significant role in resolving this apparent contradiction. Finally, it is interesting to consider also the total energies released in the X-ray band during the observed IXPs. We find $< \log_{10} E_{IXP,iso}[s] >= 49.5$, $\sigma_{\log_{10}(E_{IXP})} = 0.9$. Taking into account the typical beaming of sGRBs (with a jet opening angle of $\theta_0 \approx 0.1$, see Beniamini et al. 2019; Nakar 2020), the collimation corrected energies corresponding to the values above are approximately two orders of magnitude lower. All together, the energies observed in IXPs are approximately five orders of magnitude below the typical energy release expected from a SMNS before collapse (see Fig. 2). Furthermore, the large spread in plateau energies is also not expected in this scenario (in contrast with the survival time, the energy release is independent of the magnetic field strength and is expected to be quite narrowly distributed). We conclude that the observed plateau data are not naturally explained by energy injection from a SMNS merger remnant.

An additional emission feature seen in $\sim 15 - 20\%$ of sGRBs is the 'extended emission' (EE; Lazzati et al. 2001; Gehrels et al. 2006; Norris et al. 2010), a prolonged feature of soft γ-rays lasting ~ 100 s after the initial prompt hard spike. Similar to IXPs, the EE terminates on a timescale that is very short relative to their overall duration (and indeed exhibit significant variability during their activity) and may therefore be an indication of SMNS collapse. 7/39 GRBs in the Gompertz et al. (2020) sample exhibit EE. Their (source frame) durations are $< \log_{10} t_{EE}[s] >= 1.85$, $\sigma_{\log_{10}(t_{EE})} = 0.16$. As for the IXPs, this distribution is much narrower than naturally expected from SMNS collapse. Furthermore, if such an association is true, EE sGRBs should result in extremely bright radio remnants (as will be discussed §4.2). Fong et al. (2016) have conducted a specific search
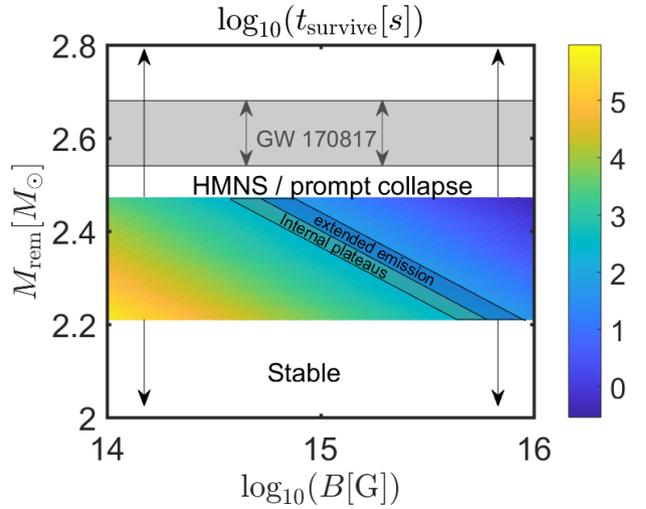

Figure 4. Survival time of a magnetar NS merger remnant as a function of the dipole field strength, B, and the gravitational mass of the remnant as it enters the phase of cold uniform rotation, M_{rem} (this is larger than the final gravitational mass, by the time the remnant has spun down). At large masses, the magnetar promptly collapses to a black hole, while at lower masses the magnetar is indefinitely stable. Finite survival times are possible in between and are very sensitive to both B and M_{rem}. As a comparison, the durations of all SGRBs with 'internal plateaus' span a narrow strip in this parameter space, denoted by a diagonal shaded region. Also shown in comparison is the remnant mass of GW170817, which favours a rapid collapse. We assume the remnant lost $0.1 - 0.2 M_\odot$ due to GW emission, neutrinos and baryonic ejecta during the merger. Results in this plot are calculated according to the procedure described in §2 and for the SLy EoS.

in radio for EE sGRBs and their search yielded only upper limits. In particular, for the EE sGRB, 050724, the ejecta energy is constrained to be $< 10^{52}$ erg, much below the energies associated with long lived NS remnants. In addition, the radio search of Ricci et al. (2021) limits the released energy of three of the other EE sGRBs in the Gompertz et al. (2020) sample: $E_{060614} < 5 \times 10^{52}$ erg, $E_{061006} < 4.5 \times 10^{52}$ erg, $E_{060614} < 3 \times 10^{52}$ erg.

4.2 EM signatures of magnetar boosted outflows

Energy ejected by the magnetar prior to the point of collapse will eventually catch up with the (roughly isotropic) ejecta expanding away from the merger remnant. This energy could then re-energize the ejecta [4] and may significantly overwhelm the initial kinetic energy of the ejecta.

Depending on the timescale of energy injection relative to the diffusion time, this process may lead to a magnetar-boosted kilonova (Kasen & Bildsten 2010; Yu et al. 2013; Metzger & Piro 2014). However, the effect of this energy injection on the radio light-curve is more generic. The peak of the radio lightcurve from the merger ejecta occurs on a timescale of years to tens of years, when the mildly relativistic ejecta has been decelerated by the external medium (Nakar & Piran 2011; Piran et al. 2013; Hotokezaka et al. 2018b; Radice et al. 2018c; Kathirgamaraju et al. 2019). This timescale is longer than $t_{survive}$ for any reasonable value of the magnetic field (that could account for the production of a GRB in the earlier stages). Furthermore,

---

[4] The extent to which this happens depends on how efficiently the injected energy is absorbed by the ejecta (see e.g. Metzger & Piro 2014)

the observed signal depends on the (narrowly distributed) kinetic energy of the ejecta and is independent of the specific time at which energy was added to the ejecta. As a result the radio counterpart is rather robust to the uncertainties in the merger outcome. The flux and duration of the peak are given by

$$F_{\nu,\text{pk}} = 200\epsilon_{e,-1}^{p-1}\epsilon_{B,-3}^{\frac{p+1}{4}}n_0^{\frac{p+1}{4}}M_{\text{ej},-1}^{\frac{7-5p}{4}}E_{51}^{\frac{5p-3}{4}}\nu_9^{\frac{1-p}{2}}d_{26}^{-2}\mu\text{Jy} \quad (6)$$

$$t_{\text{pk}} = 3.5 n_0^{-1/3} E_{51}^{-1/2} M_{\text{ej},-1}^{5/6} \text{ yr} \quad (7)$$

where E is the energy of the blastwave, n is the external density, d is the distance of the explosion, ϵ_e, ϵ_B are the fractions of the shock energy, deposited in relativistic electrons / magnetic fields respectively, p is the index of the shocked electrons' PL energy distribution and M_{ej} is the total ejecta mass. The numerical coefficients in Eq. 6 depend in general on p, α (where α describes the distribution of velocities in the ejecta, $E(>\beta\Gamma) \propto (\beta\Gamma)^{-\alpha}$) and are estimated here for $p \approx 2.2, \alpha \approx 4$ (e.g. Nakar & Piran 2017; Kathirgamaraju et al. 2019). This choice of α corresponds to a steep energy profile, meaning that the results are weakly dependent on its exact value, and deriving the same expressions assuming only a single velocity to the ejecta would only have introduced an order unity change. We also employ the convention $q_X \equiv q/10^X$ in cgs units (except for M_{ej} which is in units of $M_\odot$). With the large values of extracted energies given in §3, we can expect a large number of such bright radio transients.

Previous studies have considered radio follow-up observations of known sGRBs years after the bursts, and limits have been put on the kinetic energies of the ejecta in those bursts (Metzger & Bower 2014; Fong et al. 2016; Horesh et al. 2016; Ricci et al. 2021). Ricci et al. (2021) found that for ejecta masses $M_{\text{ej}} < 10^{-2}M_\odot$ ($M_{\text{ej}} < 5 \times 10^{-2}M_\odot$), extracted energies $> 5 \times 10^{52}$erg ($> 10^{53}$erg) can be ruled out in all of the 17 bursts studied. If sGRBs require a black hole central engine, then it is not surprising that the ejecta kinetic energy is much below 3×10^{52} erg. However, if there is a long-lived SMNS in a large fraction of sGRBs, we would have expect larger energies (see figure 5).

An independent approach would be to look for bright radio transients in a blind survey (Metzger et al. 2015b). We calculate the number of sources (all-sky) above a given flux, resulting from mergers with different EoS and with extracted energy and ejecta mass distributions following our results in §3 as

$$N(> F_\nu) = \int \int \frac{d\mathcal{R}(z)}{dM_{\text{ej}}} \frac{t(F_\nu|M_{\text{ej}},z)}{1+z} \frac{dV}{dz} dM_{\text{ej}} dz. \quad (8)$$

where $d\mathcal{R}(z)/dM_{\text{ej}}$ is the co-moving rate of mergers with ejecta mass M_{ej} and $t(F_\nu|M_{\text{ej}},z)$ is the duration over which a merger with ejecta mass M_{ej} and from redshift z will reside above a flux F_ν. The factor of $1+z$ in the denominator is in order to convert from the co-moving to the observed rates and dV/dz is the change in a co-moving volume element with the redshift. The redshift dependence of the merger rate is obtained by convolving the cosmic star-formation rate (Madau & Dickinson 2014) with the delay time distribution between binary formation and merger, found from Galactic binary neutron stars (Beniamini & Piran 2019). The normalization for the rate of mergers is taken as $\mathcal{R} = 320$ Gpc^{-3} yr^{-1}, in line with the most recent constraints from LIGO-VIRGO (The LIGO Scientific Collaboration et al. 2020). Finally, we have taken advantage of the fact that for a given EoS, the extracted energy is to a good approximation dictated uniquely by the ejecta mass (roughly $E \propto M_{\text{ej}}^{3.2}$ for SLy and $E \propto M_{\text{ej}}^{1.2}$ for WFF2, see appendix A). In both cases the scaling holds above a minimum M_{ej} for which the production of a SMNS is possible, see §3).

In Fig. 5 we plot the results for the all-sky rates. We assume the merger remnant to be initially spinning at the mass shedding limit. We also take relatively conservative choices for the values of the microphysical parameters, $\epsilon_{e,-1} = \epsilon_{B,-3} = 1$ and the external density, $n_0 = 10^{-2}$. We note that since sGRBs result from BNS mergers (which themselves are delayed relative to star formation), they occur in lower external densities than lGRBs. Nonetheless, O'Connor et al. (2020) have recently studied sGRB afterglows and found that the majority of sGRBs take place at environments with $n \gtrsim 10^{-2.5}$ cm^{-3} (consistent also with the relatively short delay times between binary formation and merger inferred from Galactic BNSs, Beniamini & Piran 2019) and some fraction at even much greater densities. With this in mind, we consider also the contribution from a 5% sub-population of BNS mergers that take place at greater external densities $n \approx 1$ cm^{-3}. At the high flux end, the curves in Fig. 5 follow to a good approximation the scaling $N(> F_\nu) \propto F^{-3/2}$ expected for standard candles in Euclidean geometry. We compare the resulting distributions with the planned sensitivities of the PiGSS, CNSS and VLASS radio surveys (Bower et al. 2010; Mooley et al. 2016; Lacy et al. 2020). Our results suggest that if BNS mergers enter the cold uniform rotation phase with a rotational energy close to that of the mass shedding limit, then their radio counterparts should be detectable by the VLASS and potentially also the CNSS surveys. This is a promising avenue towards testing the nature of the remnants of BNS mergers.

At times greater than t_{pk}, the kilonova ejecta's velocity becomes dependent only on the blastwave energy and not on its mass. Thus, once the ejecta slows down to Newtonian velocities, the emission becomes very similar to that of a supernova remnant. On the one hand, this is a drawback, as simply by virtue of their rates, there are $\sim 10^3$ times more "garden variety" supernova remnants than there are kilonova (or magnetar boosted kilonova) remnants. However, these older kilonova remnants are also several orders of magnitude more common than the years old kilonova afterglow transients mentioned above. This means that there could be many such sources even in our own Galaxy or in the local group (the latter may be preferable, as the remnants will cover a smaller area of the sky and their distance can be well determined independently of their angular size). This could be extremely constraining regarding the fate of BNS mergers, provided that these remnants can be reliably identified. A full exploration of this idea is deferred to a future work. That being said, we briefly illustrate here the viability of such an endeavour. Consider a remnant that is $t = 10^5$ yrs old. Given the Galactic BNS merger rate of ~ 30 Myr^{-1} (Hotokezaka et al. 2018a) and the mass of M31, relative to our Galaxy, there should be several such sources in M31. Assuming an overall energy in the blastwave of $\sim 3 \times 10^{52}$ erg (typical of a SMNS remnant, see §3) and an ISM density of 0.1 cm^{-3}, these sources should be in the Sedov Taylor phase (rather than the latter "radiative" phase, see, e.g. Barniol Duran et al. 2016 and references therein). The integrated synchrotron flux can then be calculated according to the "deep Newtonian" formulation (Sironi & Giannios 2013). At 1 GHz, and taking $\epsilon_e = 0.1$, $\epsilon_B = 0.01$, we find $F_\nu = 5$ mJy. The radius of this remnant is approximately 100 pc, corresponding to an angular size of ~ 0.3 arcmin. The surface brightness is therefore 12 mJy arcmin^{-2}, making it potentially detectable by several existing and planned radio surveys such as NVSS, SUMSS, WODAN and EMU (Intema et al. 2017). The main challenge of such a search would be to reliably infer the energy, independently of $n, \epsilon_e, \epsilon_B$. If this can be done, then a remnant with an estimated energy $\gtrsim 3 \times 10^{52}$ erg would be a "smoking gun" evidence of a BNS remnant that produced a long lived magnetar. Conversely, if the existence of such energetic
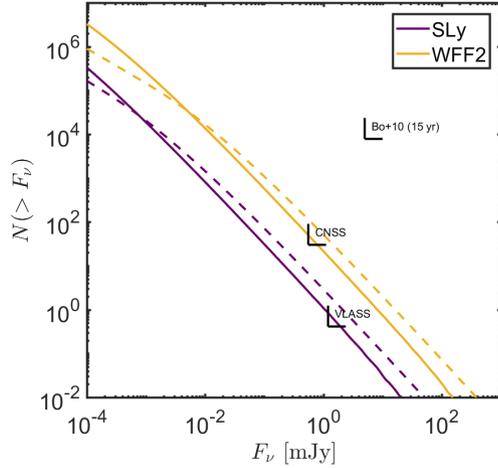
Figure 5. The all-sky number of radio sources above a given flux threshold. Results are shown for an observed frequency of 3 GHz, as well as for $\epsilon_e = 10^{-1}$, $\epsilon_B = 10^{-3}$. Solid lines are depict an external density $n = 10^{-2}$ cm^{-3} for the entire population, while dashed lines show the potential contribution assuming a small fraction of the BNS mergers (taken here as 5%) occur at an external density of $n = 1$ cm^{-3}. The extracted energy and ejecta mass distributions correspond to the two EoSs explored in this work, under the assumption that the remnant enters the phase of cold uniform rotation at the mass shedding limit. As a comparison we show sensitivity limits of different (planned) surveys (Bower et al. 2010; Mooley et al. 2016; Lacy et al. 2020).

remnants can be ruled out, it would favour remnants that collapse early on to form black holes.

5 CONCLUSIONS AND DISCUSSION

We have explored in this work the expected outcome of binary NS-NS mergers as informed by the Galactic BNS population, numerical relativity merger simulations and current constraints on the NS EoS. We assume that a NS merger remnant can cool down and lose differential rotation within the first $\sim 0.3 - 1$ s after the merger. Using models of cold and uniformly rotating NSs we calculate the evolution of the merger remnants after this initial phase (we return to the validity of this assumption below). We find that a significant fraction of mergers $(0.45 - 0.9)$ are expected to end up as SMNS which would survive for finite times before collapsing. The survival time is typically dominated by the dipole spin-down time (the mean survival time is roughly 35% of the spin-down time, corresponding to the mean fraction of rotational energy that needs to be lost before the NS collapses) and its value strongly depends on the final remnant mass and dipole field strength. Even for a fixed dipole field strength between merger remnants, the scatter in the survival time distributions is rather large, with $\sigma_{\log_{10} t_{\text{survive}}} = 0.5$. If a SMNS is formed, a large amount of energy, $\sim 10^{52} - 10^{53}$ erg, is extracted from the NS before it becomes unstable and undergoes collapse.

This abruptly terminating energy source has previously been invoked to explain IXPs (internal X-ray plateaus - in which the flux stays roughly constant and then declines very rapidly) seen in short GRB afterglow lightcurves. However, we find that the distribution of observed IXP durations is very narrow while the distribution of released energy in IXPs is very wide. Both behaviours are the opposite to what would be expected from a SMNS collapse and the

comparison of the model with observations strongly disfavours the interpretation of energy injection from a pre-collapse SMNS.

The huge amount of energy injected to the blastwave before the SMNS collapses, leads to extremely bright radio transients (due to deceleration of the sub-relativistic ejecta by the surrounding environment). Such sources have already previously been ruled out in all 17 short GRBs in which deep searches have been carried out (Ricci et al. 2021). Furthermore, we calculate here the all-sky rate of such sources and find that at 3 GHz, $1 \lesssim N(> 1 \text{ mJy}) \lesssim 50$ sources are expected. This can be put to the test with existing and future radio surveys. The advantage of this technique over follow-ups of specific GRBs, is that it can constrain also the possibility that the mergers that lead to SMNSs (that inject a large amount of energy to a sub-relativistic outflow) are preferentially those that do not lead to GRBs. Such a trend is reasonable considering that simulations of BNS mergers find unfavourable conditions for the formation of an ultra-relativistic jet (as required for powering GRBs) in cases where a long lived NS is formed (Ciolfi et al. 2019).

An independent line of reasoning stems from the typical time intervals between the binary merger and the launch of a sGRB jet. Beniamini et al. (2020b) have studied sGRBs with known redshift and shown that the jet-launching delay is typically $\lesssim 0.1$ s. These results are inconsistent with expectations from the model where sGRBs are powered by long-lived rapidly rotating NSs instead of black hole accretion. The reason is that shortly after its formation, the environment surrounding the magnetar is very baryon rich, preventing the formation of an ultra-relativistic jet, as required for powering the GRB prompt emission (see Beniamini et al. 2017 for details). For values of the dipole field consistent with powering short GRBs $(\sim 10^{15} - 10^{16} \text{ G})$ the pulsar wind achieve high magnetization (and hence high Lorentz factor) only after a delay of $\gtrsim 10$ s, which is significantly longer than the values inferred from observed sGRBs $(\lesssim 0.1 \text{ s}$, as mentioned above).

All three lines of evidence (IXP, radio afterglow, and jet launching time) shed serious doubts on the formation of long-lived or indefinitely stable magnetars from BNS mergers. This, however, appears to be inconsistent with the estimates of large fractions of such outcomes mentioned at the head of this section. We propose that all these pieces of information can be consistently resolved if merger remnants tend to collapse early on after the merger — while the proto-NS is still undergoing differential rotation and/or neutrino cooling. This can be tested in the future with detailed GRMHD simulations of differentially rotating NSs with neutrino cooling. Although such a calculation is beyond the scope of this work, we roughly outline below why such an outcome is at least plausible.

After GW emission becomes unimportant, the remnant has a slowly rotating core and rapidly rotating envelope (e.g., Kiuchi et al. 2014; Hanauske et al. 2017; Ciolfi et al. 2019). The angular frequency Ω increases with circumferential radius r until a maximum is reached, and then the rotational rate gradually drops and asymptotically approaches the Keplerian rate at large radii. Such a differentially rotating system can be divided into two regions: (1) in the outer region where $d\Omega/dr < 0$, the magneto-rotational instability (MRI, Balbus & Hawley 1998) generates strong MHD turbulence/dissipation and hence leads to efficient transport of angular momentum; (2) in the inner region where $d\Omega/dr > 0$, MRI does not operate, but the free energy associated with differential rotation is spent to amplify the toroidal magnetic field which grows and saturates due to non-linear dissipation — such energy dissipation tends to push the system towards uniform rotation, because the system has the general tendency of evolving towards the minimum energy state (Lynden-Bell & Pringle 1974). However, the mechanism for magnetic energy

dissipation as well as the dissipation rate is currently unknown (the dissipation in above-mentioned simulations are largely due to numerical viscosity).

The magnetic energy dissipation timescale may be written as some multiplicity factor $\xi > 1$ times the Alfvén crossing time $t_A \sim \sqrt{4\pi\rho R^2}/B_\phi \sim 10$ ms $B_{\phi,16}^{-1}$, where we have taken $\rho \sim 10^{15}$ g cm^{-3} for the typical core density, a NS radius $R \sim 10$ km, and a toroidal field strength $B_\phi = 10^{16} B_{\phi,16}$ G. On a timescale ξt_A, the magnetic energy associated with the toroidal fields $E_B = (1/6) B_\phi^2 R^3$ is dissipated, giving rise to a dissipation rate of $\dot{E}_B = E_B/(\xi t_A)$. If the free energy associated with differential rotation is $E_{dr} \sim 10^{53}$ erg, then the timescale for removing differential rotation is given by $t_{diff} \sim E_{dr}/\dot{E}_B \sim (70\,\text{s}) \xi E_{dr,53} B_{\phi,16}^{-3}$. We see that, even for a conservative choice of $\xi \sim 1$, $B_\phi \gtrsim 10^{17}$ G is required to remove the differential rotation in 0.1 s (i.e. to *increase* the rotation rate of the inner core to that of the outer regions). Such a strong magnetic field is energetically possible (Ciolfi et al. 2019), but it may inevitably lead to a very large viscosity in the outer region (where the density is much lower) and to rapid spin-down of the remnant. Stability of the magnetic configuration in the NS interior requires a minimum poloidal-to-toroidal field ratio , $B_p/B_\phi \gtrsim 3(E_B/E_{grav})^{1/2}$, where $E_{grav} \sim 10^{54}$ erg is the gravitational binding energy (Akgün et al. 2013). This sets a minimum poloidal field $B_p \gtrsim 10^{16}$ G, which would still cause the remnant to spin down in less than a few seconds (see the bottom panel of Fig. 2).

The consequence may be that, before the inner core is spun up, most of the energy dissipation occurs in the MRI-dominated outer region and that the majority of the angular momentum is rapidly transported to large radii $\gg 10$ km. In that case, the mass added to the core has a specific angular momentum that is smaller than the minimum angular momentum of a uniformly rotating SMNS of the same mass. Accretion of low angular momentum gas, along with neutrino cooling, will increase the central density (Kaplan et al. 2014), so it is possible that the remnant collapses to a black hole because the rotation energy is much less than the mass shedding limit $E_\Omega \ll E_{\Omega,max}$ (as discussed in §3.1). After the collapse, the gas with larger specific angular momentum than that of the black hole, but less than that of the innermost stable orbit, will quickly plunge into the black hole. The outermost layers will then slowly accrete onto the black hole and power a GRB jet.

Finally, we note that our results supporting a black hole central engine powering short GRBs may also be extendable to long GRBs. The chief reason being the similarity in many of the observed properties between the two types of GRBs (e.g. in terms of the luminosities, the bulk Lorentz factors and the prompt GRB light curve morphology and spectral shape). Occam's razor would suggest that the simplest explanation is that they share a central engine and jet launching mechanism. An additional consideration is the total mass involved in a stellar collapse leading to a long GRB, which could apriori easily exceed M_{max} and lead to a proto-NS that would not remain stable for long enough to power the observed GRB.

REFERENCES

Akgün T., Reisenegger A., Mastrano A., Marchant P., 2013, MNRAS, 433, 2445
Antoniadis J., et al., 2013, Science, 340, 448
Baiotti L., Giacomazzo B., Rezzolla L., 2008, Phys. Rev. D, 78, 084033
Balbus S. A., Hawley J. F., 1998, Reviews of Modern Physics, 70, 1
Barniol Duran R., Whitehead J. F., Giannios D., 2016, MNRAS, 462, L31
Beniamini P., Piran T., 2019, MNRAS, 487, 4847
Beniamini P., Giannios D., Metzger B. D., 2017, MNRAS, 472, 3058
Beniamini P., Petropoulou M., Barniol Duran R., Giannios D., 2019, MNRAS, 483, 840
Beniamini P., Duque R., Daigne F., Mochkovitch R., 2020a, MNRAS, 492, 2847
Beniamini P., Duran R. B., Petropoulou M., Giannios D., 2020b, ApJ, 895, L33
Bernuzzi S., Radice D., Ott C. D., Roberts L. F., Mösta P., Galeazzi F., 2016, Phys. Rev. D, 94, 024023
Bower G. C., et al., 2010, ApJ, 725, 1792
Breu C., Rezzolla L., 2016, MNRAS, 459, 646
Cameron A. D., et al., 2018, MNRAS, 475, L57
Champion D. J., et al., 2005, MNRAS, 363, 929
Ciolfi R., Kastaun W., Kalinani J. V., Giacomazzo B., 2019, Phys. Rev. D, 100, 023005
Cook G. B., Shapiro S. L., Teukolsky S. A., 1994, ApJ, 424, 823
Coughlin M. W., Dietrich T., Margalit B., Metzger B. D., 2019, MNRAS, 489, L91
Cromartie H. T., et al., 2020, Nature Astronomy, 4, 72
Dall'Osso S., Stratta G., Guetta D., Covino S., De Cesare G., Stella L., 2011, A&A, 526, A121
Demorest P. B., Pennucci T., Ransom S. M., Roberts M. S. E., Hessels J. W. T., 2010, Nature, 467, 1081
Douchin F., Haensel P., 2001, A&A, 380, 151
Eichler D., Granot J., 2006, ApJ, 641, L5
Faulkner A. J., et al., 2005, ApJ, 618, L119
Fong W., Metzger B. D., Berger E., Özel F., 2016, ApJ, 831, 141
Fujibayashi S., Kiuchi K., Nishimura N., Sekiguchi Y., Shibata M., 2018, ApJ, 860, 64
Gao H., Ding X., Wu X.-F., Zhang B., Dai Z.-G., 2013, ApJ, 771, 86
Gehrels N., et al., 2006, Nature, 444, 1044
Genet F., Daigne F., Mochkovitch R., 2007, MNRAS, 381, 732
Giacomazzo B., Perna R., 2013, ApJ, 771, L26
Gompertz B. P., Levan A. J., Tanvir N. R., 2020, ApJ, 895, 58
Granot J., Königl A., Piran T., 2006, MNRAS, 370, 1946
Granot J., Guetta D., Gill R., 2017, ApJ, 850, L24
Hanauske M., Takami K., Bovard L., Rezzolla L., Font J. A., Galeazzi F., Stöcker H., 2017, Phys. Rev. D, 96, 043004
Horesh A., Hotokezaka K., Piran T., Nakar E., Hancock P., 2016, ApJ, 819, L22
Hotokezaka K., Kiuchi K., Kyutoku K., Muranushi T., Sekiguchi Y.-i., Shibata M., Taniguchi K., 2013, Phys. Rev. D, 88, 044026
Hotokezaka K., Beniamini P., Piran T., 2018a, International Journal of Modern Physics D, 27, 1842005
Hotokezaka K., Kiuchi K., Shibata M., Nakar E., Piran T., 2018b, ApJ, 867, 95
Intema H. T., Jagannathan P., Mooley K. P., Frail D. A., 2017, A&A, 598, A78
Ioka K., Toma K., Yamazaki R., Nakamura T., 2006, A&A, 458, 7
Janssen G. H., Stappers B. W., Kramer M., Nice D. J., Jessner A., Cognard I., Purver M. B., 2008, A&A, 490, 753
Kaplan J. D., Ott C. D., O'Connor E. P., Kiuchi K., Roberts L., Duez M., 2014, ApJ, 790, 19
Kasen D., Bildsten L., 2010, ApJ, 717, 245
Kathirgamaraju A., Giannios D., Beniamini P., 2019, MNRAS, 487, 3914
Kiuchi K., Kyutoku K., Sekiguchi Y., Shibata M., Wada T., 2014, Phys. Rev. D, 90, 041502
Kiuchi K., Kyutoku K., Sekiguchi Y., Shibata M., 2018, Phys. Rev. D, 97, 124039

Kramer M., et al., 2006, Science, 314, 97
Lacy M., et al., 2020, PASP, 132, 035001
Lazarus P., et al., 2016, ApJ, 831, 150
Lazzati D., Ramirez-Ruiz E., Ghisellini G., 2001, A&A, 379, L39
Lorimer D. R., et al., 2006, ApJ, 640, 428
Lynch R. S., et al., 2018, ApJ, 859, 93
Lynden-Bell D., Pringle J. E., 1974, MNRAS, 168, 603
Madau P., Dickinson M., 2014, ARA&A, 52, 415
Margalit B., Metzger B. D., 2017, ApJ, 850, L19
Margalit B., Metzger B. D., 2019, ApJ, 880, L15
Martinez J. G., et al., 2015, ApJ, 812, 143
Metzger B. D., Bower G. C., 2014, MNRAS, 437, 1821
Metzger B. D., Piro A. L., 2014, MNRAS, 439, 3916
Metzger B. D., Giannios D., Thompson T. A., Bucciantini N., Quataert E.,
    2011, MNRAS, 413, 2031
Metzger B. D., Margalit B., Kasen D., Quataert E., 2015a, MNRAS, 454,
    3311
Metzger B. D., Williams P. K. G., Berger E., 2015b, ApJ, 806, 224
Metzger B. D., Beniamini P., Giannios D., 2018, ApJ, 857, 95
Mooley K. P., et al., 2016, ApJ, 818, 105
Nakar E., 2020, Phys. Rep., 886, 1
Nakar E., Piran T., 2011, Nature, 478, 82
Nakar E., Piran T., 2017, ApJ, 834, 28
Norris J. P., Gehrels N., Scargle J. D., 2010, ApJ, 717, 411
O'Connor B., Beniamini P., Kouveliotou C., 2020, MNRAS, 495, 4782
Oganesyan G., Ascenzi S., Branchesi M., Salafia O. S., Dall'Osso S.,
    Ghirlanda G., 2020, ApJ, 893, 88
Piran T., Nakar E., Rosswog S., 2013, MNRAS, 430, 2121
Radice D., 2017, ApJ, 838, L2
Radice D., Perego A., Bernuzzi S., Zhang B., 2018a, MNRAS, 481, 3670
Radice D., Perego A., Hotokezaka K., Fromm S. A., Bernuzzi S., Roberts
    L. F., 2018b, ApJ, 869, 130
Radice D., Perego A., Hotokezaka K., Fromm S. A., Bernuzzi S., Roberts
    L. F., 2018c, ApJ, 869, 130
Rezzolla L., Kumar P., 2015, ApJ, 802, 95
Rezzolla L., Most E. R., Weih L. R., 2018, ApJ, 852, L25
Ricci R., et al., 2021, MNRAS, 500, 1708
Rowlinson A., et al., 2010, MNRAS, 409, 531
Sekiguchi Y., Kiuchi K., Kyutoku K., Shibata M., 2011, Phys. Rev. Lett., 107,
    051102
Shakura N. I., Sunyaev R. A., 1973, A&A, 500, 33
Shen R., Matzner C. D., 2012, ApJ, 744, 36
Shibata M., Hotokezaka K., 2019, Annual Review of Nuclear and Particle
    Science, 69, 41
Shibata M., Taniguchi K., 2006, Phys. Rev. D, 73, 064027
Shibata M., Kiuchi K., Sekiguchi Y.-i., 2017a, Phys. Rev. D, 95, 083005
Shibata M., Fujibayashi S., Hotokezaka K., Kiuchi K., Kyutoku K., Sekiguchi
    Y., Tanaka M., 2017b, Phys. Rev. D, 96, 123012
Sironi L., Giannios D., 2013, ApJ, 778, 107
Stairs I. H., Thorsett S. E., Taylor J. H., Wolszczan A., 2002, ApJ, 581, 501
Stergioulas N., Friedman J. L., 1995, ApJ, 444, 306
Stovall K., et al., 2018, ApJ, 854, L22
The LIGO Scientific Collaboration et al., 2020, arXiv e-prints, p.
    arXiv:2010.14533
Weisberg J. M., Nice D. J., Taylor J. H., 2010, ApJ, 722, 1030
Wiringa R. B., Fiks V., Fabrocini A., 1988, Phys. Rev. C, 38, 1010
Yu Y.-W., Zhang B., Gao H., 2013, ApJ, 776, L40
Zhang B., 2013, ApJ, 763, L22
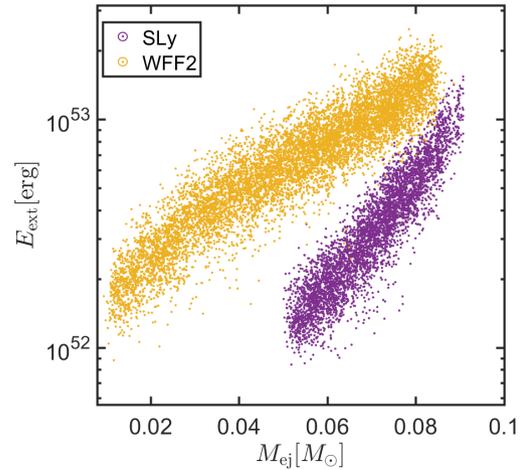Zhang B., Mészáros P., 2001, ApJ, 552, L35

Figure A1. Extracted energies as a function for ejecta masses for the two EoSs used in this paper assuming the remnant is initially rotating at the mass shedding limit. The data here is shown for systems that produce SMNS or stable NSs. Lower ejecta masses (leading to HMNS or prompt collapse) are possible, but are not associated with a significant extracted energy, and therefore not seen in this figure.

This paper has been typeset from a TeX/LaTeX file prepared by the author.

APPENDIX A: DISTRIBUTION OF EJECTA MASSES AND EXTRACTED ENERGIES

The distribution of extracted energies and ejecta masses for the EoSs used in this work are presented in figure A1.